First detection of a "minor" elevated stratopause in very early winter

Maya García-Comas[1], Bernd Funke, Manuel López-Puertas, Francisco González-Galindo[1], Michael Kiefer [2], Michael Höpfner [2]

[1]Instituto de Astrofísica de Andalucía (CSIC), Glorieta de la Astronomía s/n, 18008 Granada, Spain.
[2]Karlsruhe Institute of Technology, Institute of Meteorology and Climate Research, Karlsruhe, Germany

Key Points:

- MIPAS and MLS observed a highly zonally asymmetric Arctic stratopause at high altitudes in November 2009 followed by a strong descent.
- The event has similarities with typical elevated stratopause events but it is of smaller scale in terms of duration and extent.
- This is the first time an elevated stratopause observed from space this early in the winter season is reported.

Corresponding author: Maia García-Comas, maya@iaa.es

Abstract

Elevated stratopauses are typically associated with prolonged disturbed conditions in the northern hemisphere polar winter. MIPAS and MLS observed a short-lived and highly zonally asymmetric stratopause at mesospheric altitudes in November 2009, the earliest in the season reported so far. The Arctic climatological winter stratopause vanished and MIPAS and MLS measured temperatures of 260K at 82 km and 250K at 75 km, respectively, in a region smaller than in typical mid-winter elevated stratopause events. Planetary wave activity was initially high. Zonal mean zonal winds and the poleward temperature gradient northward of 70°N stayed reversed during 7 days. The mesosphere did not cool during that phase. Wave activity dropped until the eastward stratospheric zonal winds resumed, a strong vortex restored in the mesosphere, and the stratopause emerged at a high altitude. An enhanced downward transport followed. It took the stratopause 9 days to move down to its typical winter altitudes.

1 Introduction

Elevated statopauses (ES), firstly reported by *Manney et al.* [2005], are known as winter phenomena normally ocurring in winter, where the polar stratopause temperature in the 20-90 km range) reforms at an altitude considerably higher (around 80 km) than its mean climatological value (50–60 km) during the recovery phase of after a sudden stratospheric warming (SSW). In a typical ES event, the temperature profile is close to isothermal from the lower stratosphere to the upper mesosphere right after the SSW. This is produced by the weakened (or reversed) westerlies in the stratosphere that reduce the upward propagation of planetary waves, blurring the climatological stratopause. When the vortex starts recovering and the mesospheric westward wave forcing resumes, it may be large enough to induce strong adiabatic heating from maximum downwelling at altitudes higher than usual. That leads to the development of a stratopause there, often called elevated stratopause. A subsequent strong air descent and lowering of the stratopause, mainly driven by a strong gravity-wave-induced diabatic descent, occur next [*Manney et al.*, 2008, 2009; *Siskind et al.*, 2010; *Ren et al.*, 2011; *Chandran et al.*, 2011; *Chandran et al.*, 2013a,b; *Hitchcock and Shepherd*, 2013; *Yamashita et al.*, 2013; *Limpasuvan et al.*, 2016; *Orsolini et al.*, 2017].

Insight into the formation and evolution of a high-altitude stratopause is relevant for several reasons. First, it is important to the understanding of energy transfer in the middle atmosphere from lower regions through wave connections. ES events can additionally affect the coupling due to gravity waves up to the thermosphere [*Yigit and Medvedev*, 2016]. Secondly, the resulting modified temperature vertical gradients affect the atmospheric stability around ESs. Thirdly, the enhanced vertical advection typically following ESs impacts the distribution of atmospheric species, further altering the chemistry of the regions below. That leads to NO_x-rich mesospheric air destroying stratospheric ozone [*Randall et al.*, 2005, 2009] and H_2O-poor air indirectly enhancing the ozone tertiary maximum [*Smith et al.*, 2009]. The sequence of events originating and associated with a typical ES is mostly understood but the detailed interaction of waves, their seasonality and their interannual variability are still under discussion.

Elevated stratopauses have mostly been observed in connection with strong and prolongued SSWs, in 2004, 2006, 2009, 2010, 2013, 2018, and 2019 [*Smith et al.*, 2009; *France and Harvey*, 2013; *Funke et al.*, 2014; *Orsolini et al.*, 2017; *Schranz et al.*, 2019], all categorized as major as for The World Meteorological Office (WMO) definition. At the time of this writing, only one ES, that of January 2012, has been observed after a warming qualifying as minor [*France and Harvey*, 2013; *Funke et al.*, 2014], that is, after a reversal of the poleward temperature gradient at 10 mb from 60°N, as in major warmings, but with no mean zonal wind reversal at 10 mb at 60°N. Despite these observational statistics, climate model simulations associate one third of all ESs with minor warmings

[*de la Torre et al.*, 2012; *Chandran et al.*, 2013a; *Holt et al.*, 2013; *Chandran et al.*, 2014]. Whether concurrent with major or minor warmings, ES events have always been observed from January to March. The Whole Atmosphere Community Climate Model (WACCM) predicts ESs preferentially from December to February [*Holt et al.*, 2013; *Limpasuvan et al.*, 2016] but also in November *France and Harvey* [2013]. There is evidence of stratospheric warmings occurring in November [*Maury et al.*, 2016; *Butler et al.*, 2017] but, to our knowledge, no ES developing that early in the season has been detected up to date.

This paper reports on the first observation of an Arctic elevated stratopause in the very early winter season. The Michelson Interferometer for Passive Atmospheric Sounding (MIPAS) registered the stratopause at 82 km in late November 2009 and a subsequent strong descent in the middle atmosphere. The Microwave Limb Sounder (MLS) also measured the ES, although at a lower altitude. The phenomenon followed a weak stratospheric warming, already catalogued in the literature but with a definition more relaxed than that of WMO [*Maury et al.*, 2016]. A mesospheric cooling associated to the warming was not measured. The middle-atmosphere temperature vertical gradients decreased after the warming, leading to an ill-defined stratopause. This ES event was shorter-lived and of smaller extension than typical mid-winter ones but it was still remarkable. What were the circumstances paving the way to this minor ES? How did the episode develop and progress? Did something peculiar happen during the very early winter of 2009? We describe here the phenomenon as seen by MIPAS and MLS and also report on the plausible preconditioning by inspecting the Modern-Era Retrospective analysis for Research and Applications, Version 2 (MERRA-2) data.

2 Data

MIPAS, onboard the ENVISAT satellite, observed the limb from 2002 to 2012 from a 10:00LT sun-synchronous polar orbit during day and night with a global coverage [*Fischer et al.*, 2008]. Its vertical coverage was usually 6-68 km (NOMinal mode, NOM) and less often 20-102 km and 40-170 km (Middle- and Upper-Atmosphere modes, MA and UA, respectively). We use here MIPAS IMK/IAA retrievals of temperature, line of sight (LOS) altitude information, CO, NO_x and H_2O in their versions V5R_220 (NOM) and V5R_m21 (MA/UA) except V5R_m22 for MA/UA H_2O [*von Clarmann et al.*, 2009; *García-Comas et al.*, 2014; *Funke et al.*, 2009; *Bermejo-Pantaleón et al.*, 2011; *Funke et al.*, 2014; *García-Comas et al.*, 2016; *Lossow et al.*, 2017]. Their vertical resolutions in the mesosphere are 4-6 km (temperature), 4-7 km (CO), 7-25 km (NO_x) and 4-6 km (H_2O). MIPAS provided upper mesosphere measurements in the very early winter of 2009 only for a few days.

A better temporal coverage in the upper mesosphere is accomplished by also using Aura's Microwave Limb Sounder (MLS). MLS provides temperature profiles since 2004 from 261 to 0.001 hPa at 82°N-82°S on a daily basis. We use version 4.2 temperatures, which supersedes v2.2 [*Schwartz et al.*, 2008], and apply the data screening described in *Livesey et al.* [2017]. MLS temperature vertical resolution is 4-6 km in the stratosphere and 6-10 km in the mesosphere.

MERRA-2 assimilation data provided the winds and potential vorticity used here [*Gelaro et al.*, 2017]. MERRA-2 utilizes an upgraded version of the Goddard Earth Observing System Model, Version 5 (GEOS-5) data assimilation system. Spatial resolution is 0.625° in longitude and 0.5° in latitude (about 50 km). We use v5.12.4 instantaneous 3-hourly fields in pressure coordinates [*Global Modeling and Assimilation Office (GMAO)*, 2015].

3 Results

Figure 1 shows stereographic maps of MIPAS temperature and height at several pressure levels from the lower stratosphere to the upper mesosphere for November 29^{th} 2009. Equivalent latitude contours at 50°N and 70°N estimated from ECMWF potential vorticity [*Dee et al.*, 2011] are overplotted. We note that equivalent latitudes drawn at 0.2 hPa and lower pressures correspond to those at 0.1 hPa.

The equivalent latitudes and the minimum altitudes at each pressure level in Fig. 1 show a vortex displaced off the pole and centered around 70-75°N geographical latitude. The vortex at 45 hPa (~20 km) was located over the Siberian northeast (135°E) (not shown). It was significantly tilted to the west as pressure decreased. At 10 hPa (~30 km), it was at 120°E, to the north of central Siberia. At 0.45 hPa (~50 km), it was located at 30°W, over Greenland. The vortex tilt above shows a close to baroclinic structure up to 0.045 hPa (~65 km). From there up, it was displaced only to 60°W at 0.004 hPa (~82 km), over the Arctic archipelago. This longitudinally asymmetric structure presented the aspect of a wave-1 perturbation at all pressure levels.

Lowest temperatures at levels below 0.2 hPa (~55 km) were offset 20-30° to the west with respect to the center of the vortex (minimum altitudes, maximum equivalent latitudes). From 0.1 hPa (~60 km) to 0.01 hPa (~75 km), highest temperatures were almost aligned with the vortex, as displayed by the altitude distribution at these pressure levels (not shown). At 0.004 hPa (~82 km), the warmest temperatures (260K) were over central Greenland, that is, they were displaced 30° to the east with respect to the lowest heights. A similar highly zonally asymmetric structure persisted in MIPAS measurements at least during November 30^{th} (not shown).

The 2009 late November stratosphere to mesosphere thermal and altitude structures shown in Fig. 1 are not typical for this time of the year. MIPAS monthly climatology, constructed using temperatures at latitudes higher than 70°N averaged from mid-November to mid-December from 2007 to 2011 except 2009 (not shown), exhibits a 260K stratopause located around 0.2hPa (~55 km). Temperature monotonically decreases above and up to around 0.0004hPa (~95 km), where a cold 180K mesopause resides. Instead, temperatures in 2009 late November increase monotonically from the lower stratopause up to 0.004 hPa (~82 km), where they reach 260K. At typical stratopause altitudes, temperatures were only 225-235K then.

Figure 2a shows MIPAS temperature time series from mid-November to mid-December 2009 averaged over 70°-90°N. The previous day that MIPAS observed the upper mesosphere was October 31^{st}, when temperatures display a typical structure in the mesosphere (not shown). Therefore, MIPAS measurements cannot provide the day in November 2009 when the ES established. MLS data complements those days when MIPAS was not measuring the upper mesosphere (Fig. 2b).

On November 17^{th}, the stratopause suffers a gentle 15K warming. Opposite to stronger warmings, the stratopause does not move down to lower altitudes but it just blurs by November 23^{rd} (a bit later in MLS data). The subsequent reduced temperature vertical gradients give the way to a 260K stratopause reformed around 82 km at least from November 29^{th} to 30^{th} according to MIPAS. MLS measures a temperature peak (240K) at 70 km already on the 28^{th}, 8-10 days after the warming, and shows slight increases in ES temperature (250K) and altitude (75 km) also during the 29^{th} to 30^{th}. Then, the stratopause moves down during the next 8-9 days to its climatological mean altitude. Subsequently, a second stronger warming starts in the stratosphere, depicted in both datasets, most likely the same one *Dörnbrack et al.* [2012]) reported. The differences between MIPAS and MLS measurements can be explained by their different vertical resolution in the mesosphere. *France and Harvey* [2013] did not report any high-altitude stratopause occurring in November

when analyzing 2004-2012 MLS zonal means measurements. This is most likely due to the high zonal asymmetry of the feature found here combined with its limited extension.

Figure 3 shows the MIPAS 2007-2011 composite (upper row) and 2009 (lower row) early winter temporal evolution in the polar vortex of carbon monoxide, water vapor and NO_x, long lived species and tracers of atmospheric dynamics. The mesospheric CO and H_2O vertical distributions do not vary significantly this early in the season, indicating that the polar wintertime downward transport is still very weak. The descent depicted in December by the contour lines in the MIPAS NO_x climatology is somehow stronger than that of CO and H_2O in the mesosphere (above ~55 km). This is related to the larger photochemical impact compared to the other species during the fall to winter transition.

Polar mesospheric MIPAS observations of CO, H_2O and NO_x reveal stronger than usual downwelling starting on November 22^{nd}-23^{rd} 2009 (Fig. 3). Air rapidly descends down to the stratosphere (estimation from contour slopes results in 1 km/day). By December 5^{th}, CO and H_2O abundances at 55 km are both 4 ppmv, factors of 2-3 larger and smaller, respectively, than the climatological averages from mid-November to mid-December. The descent associated with the ES in 2009 shown by NO_x is undoubtedly stronger than that in the climatology. We note that the climatological background NO_x abundance is larger than in 2009 because 2009 was close to solar minimum [*Funke et al.*, 2014]. The mesospheric NO_x increase by December 5^{th} with respect to values at the beginning of the time series is 40% larger than in the MIPAS climatology.

Signatures of descent from the mesosphere abruptly cease by December 10^{th} 2009, in concurrence with the onset of the second warming. A tongue of CO-rich and dry air keeps progressing in the stratosphere down to 40 km until the 19^{th}. This shape points to a supply of CO-poor and wetter air around 50 km from lower latitudes, which is further supported when inspecting MIPAS horizontal maps (not shown). That supply is probably favoured by the second weakening of the vortex that also inhibits the descent of mesospheric air.

4 Discussion

In order to identify the triggers of this phenomenon, we inspected the 2009 very early winter time evolution of planetary wave activity, horizontal winds and Ertel's potential vorticiy. The upper panel of Fig. 4 shows the time series of the longitudinal wavenumber-1 (WN1) amplitudes of MIPAS height anomaly at 10 mb (~35 km) at northern latitudes. These depict the planetary wave activity in the mid-stratosphere. These were calculated by fitting wavenumbers 1 and 2 components for 10°-wide latitude boxes. Results for wavenumber-2 (WN2) are not shown because WN1 clearly dominated the planetary wave spectrum during this period. The lower panel in Fig. 4 shows the time series of MERRA-2 zonal mean zonal wind at 80°N. Figure 5 shows North hemisphere surfaces of MERRA-2 Ertel's potential vorticity in the mid-stratosphere (10 mb~35 km) and the low mesosphere (0.1 mb~65 km), respectively, for selected days.

Before November 15^{th}, winds at 80°N were eastward (Fig. 4, lower panel) and the usual early winter stratospheric polar vortex was already built up, slightly displaced to Northern Europe (Fig. 5, upper row, left column). WN1 exhibits a not very strong but continuous activity (Fig. 4).

From November 15^{th} to 17^{th}, the zonal mean zonal wind reversed at 80°N and 0.3-0.1 mb (~55-65 km; Fig. 4) but remained eastward at latitudes lower than 70°N (not shown). The 80°N winds at levels below 0.3 mb slightly decelerated. Two anticyclones had developed in the stratosphere (10 mb) over Canada and the Bering Sea and the vortex shape was perturbed both in the stratosphere and the mesosphere (2^{nd} row of Fig. 5). *Colucci and Ehrmann* [2018] reported the generation of the Aleutian High at that time. WN1 activity dropped those days, in agreement with a plausible filtering out by these two

well-defined and strong anticyclones. The lower mesosphere 80°N westward wind turned back to eastward the 17^{th} so that winds at all pressures analyzed were eastward during the following week. In parallel, WN1 resumed and intensified until the 22^{nd} and the vortex weakened once again.

By the 22^{th}, the mean zonal wind reversed to westward at altitudes below the 7 mb level but only weakly (<7 m/s) and WN1 severely dropped. The poleward zonal mean temperature gradient at 10 mb was positive but only from 70°N and only for one day, the 22^{th}, and winds south of 70°N remained eastward (not shown). This means that this stratospheric warming would not even be categorized as minor according to WMO definition.

The lower-stratospheric zonal winds at 80°N remained reversed 7 days, until the 29^{th}. In the meanwhile, the eastward winds at levels above 7 mb steadily strengthened, starting at the highest altitudes (Fig. 4, lower panel). The lower row of Figure 5 shows that, while the vortex was still distorted in the stratosphere by the 30^{th} (left), it was strong and displaced to the North of the Atlantic Ocean in the mesosphere (right). At that time, the ES was already formed (see Fig. 2) and the mean winds were eastward at all pressure levels (Fig. 4). Note that, at the end of the first week of December, the WN1 activity increased again and the mean winds became westward, initially in the mesosphere and later in the stratosphere. That was associated with the second warming mentioned above.

This sequencing of phenomena, despite the absence of significant mesospheric cooling before the ES, mostly follows that of typical elevated stratopause events [*Manney et al.*, 2008, 2009]. However, the duration of its different phases and their extent are smaller. The polar vortex in late fall and early winter is less variable than in the mid-winter [*Manney et al.*, 2002, and references therein], but the perturbations of the stratosphere in mid-November 2009 were stronger than usual for a short time. Indeed, the catalogue of *Maury et al.* [2016] (see their Fig. 5), who advise a more relaxed stratospheric warming definition than that of WMO, lists a weak stratospheric warming previous to our ES. Nonetheless, the stratopause did not move down in altitude after the warming. Yet, the vortex was critically weakened for about a week and it strongly recovered afterwards, starting in the middle mesosphere and triggering the ES. Interestingly, the circumstances that followed this warming were exceptional not only in the mesosphere. *Wang and Chen* [2010] pointed out that the perturbed 2009 November stratospheric conditions were responsible for the following December extreme cold weather over Europe, although the stronger warming at the beginning of December could also contribute [*Dörnbrack et al.*, 2012]. This work shows that this moderate stratospheric anomalies propagate not only to the surface but also to the mesosphere.

5 Conclusions

The variability of the Northern Hemisphere polar vortex in very early winter can lead to exceptional events from the troposphere to the mesosphere (and plausibly higher up). Models have reported the possibility for elevated stratopauses to develop in early winter (November and December) but these have never been observed in the past. MIPAS and MLS detected a short-lived mesoscale elevated stratopause in November 2009, the earliest in the winter season observed so far.

A region of anomalously high temperatures (260K) at high mesopause altitudes (82 km) stands out in MIPAS measurements on November 29^{th} and 30^{th}. MLS also captured this feature, although at slightly lower temperatures (250K) and altitude (75 km). Temperatures and their vertical gradients at altitudes below and down to the tropopause were significantly smaller than usual. This high altitude stratopause lived for 2-5 days. It then descended to its typical early-winter altitude (55 km) in 9-10 days; that is at least twice as rapidly as previously reported typical ESs [Fig. 13 in *Funke et al.*, 2014]. The

episode was highly longitudinally asymmetric and of small extension and, consequently, hard to detect when inspecting zonal averages. The asymmetry of elevated stratopauses has been reported previously in the literature [*France and Harvey*, 2013].

This elevated stratopause was followed by a strong vertical descent, depicted by the time evolution of several tracers. MIPAS shows that NO_x- and CO-rich and dry mesospheric air was transported down to stratospheric altitudes significantly faster (1 km/day) than usual at this time of the year. Carbon monoxide and water vapor abundances in the upper stratosphere were factors of 2-3 larger and smaller, respectively, than the climatological monthly averages in very early winter. The NO_x enhancement was 40% larger.

This high-altitude stratopause was preceded by a sequence of phenomena of smaller magnitude and less prolonged than those characteristic of typical ES events [*Manney et al.*, 2008]. In this case, planetary wave activity initially increased, in mid-November 2009. The mean zonal winds in the mid-low stratosphere reversed during one week only at 70°N. The zonal mean temperature poleward gradient was positive only at 70°N and only for one day. The mesosphere did not cool before the ES. Nonetheless, the polar vortex was critically disturbed by two anticyclones that displaced it off the pole. The planetary wave activity decreased and the climatological stratopause blurred. This situation paved the way to the reformation of a well shaped and strong vortex at high altitudes and the emergence of an elevated stratopause of smaller extension and less persistent than typically.

WACCM predicts ES events in very early winter, although *France and Harvey* [2013] and *France et al.* [2015] noted unrealistically large planetary wave amplitudes in the model. While WACCM data may overestimate planetary wave activity and over-predict ES occurrence, our results show that at least short-lived and small-size events leading to enhanced mesospheric descent can occur in November. Further work is needed in order to evaluate the ability of chemistry-climate models to reproduce a 'minor' elevated stratopause like this one. Its high zonal asymmetry, its reduced extension and its short life may be an even more stringent test for model simulations than typical ES events.

Acknowledgments

The IAA team acknowledges financial support from the State Agency for Research of the Spanish MCIU through project ESP2017–87143-R, the "Center of Excellence Severo Ochoa" award to the IAA-CSIC (SEV-2017-0709), and EC FEDER funds. MIPAS datasets can be accessed upon request at https://www.imk-asf.kit.edu/english/308.php. We thank the Global Modeling and Assimilation Office for providing MERRA-2 data and the MLS science and data processing teams for providing MLS data publicly through the NASA Goddard Space Flight Center Earth Sciences (GES) Data and Information Services Center.

References

Bermejo-Pantaleón, D., B. Funke, M. López-Puertas, M. García-Comas, G. P. Stiller, T. von Clarmann, A. Linden, U. Grabowski, M. Höpfner, M. Kiefer, N. Glatthor, S. Kellmann, and G. Lu (2011), Global Observations of Thermospheric Temperature and Nitric Oxide from MIPAS spectra at 5.3 μm, *J. Geophys. Res.*, *116*, A10313, doi: 10.1029/2011JA016752.

Butler, A. H., J. P. Sjoberg, D. J. Seidel, and K. H. Rosenlof (2017), A sudden stratospheric warming compendium, *Earth System Science Data*, *9*, 63–76, doi:10.5194/essd-9-63-2017.

Chandran, A., R. L. Collins, R. R. Garcia, and D. R. Marsh (2011), A case study of an elevated stratopause generated in the whole atmosphere community climate model, *Geophys. Res. Lett.*, *38*(8), doi:10.1029/2010GL046566, l08804.

Chandran, A., R. L. Collins, R. R. Garcia, D. R. Marsh, V. L. Harvey, J. Yue, and L. de la Torre (2013a), A climatology of elevated stratopause events in the whole

atmosphere community climate model, *J. Geophys. Res.*, *118*(3), 1234–1246, doi: 10.1002/jgrd.50123.

Chandran, A., R. R. Garcia, R. L. Collins, and L. C. Chang (2013b), Secondary planetary waves in the middle and upper atmosphere following the stratospheric sudden warming event of January 2012, *Geophysical Research Letters*, *40*, 1861–1867, doi: 10.1002/grl.50373.

Chandran, A., R. L. Collins, and V. L. Harvey (2014), Stratosphere-mesosphere coupling during stratospheric sudden warming events, *Advances in Space Research*, *53*, 1265–1289, doi:10.1016/j.asr.2014.02.005.

Colucci, S. J., and T. S. Ehrmann (2018), Synoptic-Dynamic Climatology of the Aleutian High, *Journal of Atmospheric Sciences*, *75*(4), 1271–1283, doi:10.1175/JAS-D-17-0215.1.

de la Torre, L., R. R. Garcia, D. Barriopedro, and A. Chandran (2012), Climatology and characteristics of stratospheric sudden warmings in the whole atmosphere community climate model, *J. Geophys. Res.*, *117*(D4), D04110, doi:10.1029/2011JD016840.

Dee, D. P., S. M. Uppala, A. J. Simmons, P. Berrisford, P. Poli, S. Kobayashi, U. Andrae, M. A. Balmaseda, G. Balsamo, P. Bauer, P. Bechtold, A. C. M. Beljaars, L. van de Berg, J. Bidlot, N. Bormann, C. Delsol, R. Dragani, M. Fuentes, A. J. Geer, L. Haimberger, S. B. Healy, H. Hersbach, E. V. Halm, L. Isaksen, P. Kallberg, M. Kahler, M. Matricardi, A. P. McNally, B. M. Monge-Sanz, J.-J. Morcrette, B.-K. Park, C. Peubey, P. de Rosnay, C. Tavolato, J.-N. Thapaut, and F. Vitart (2011), The era-interim reanalysis: configuration and performance of the data assimilation system, *Quart. J. Roy. Meteor. Soc.*, *137*(656), 553–597, doi:10.1002/qj.828.

Dörnbrack, A., M. C. Pitts, L. R. Poole, Y. J. Orsolini, K. Nishii, and H. Nakamura (2012), The 2009-2010 Arctic stratospheric winter - general evolution, mountain waves and predictability of an operational weather forecast model, *Atmospheric Chemistry & Physics*, *12*(8), 3659–3675, doi:10.5194/acp-12-3659-2012.

Fischer, H., M. Birk, C. Blom, B. Carli, M. Carlotti, T. von Clarmann, L. Delbouille, A. Dudhia, D. Ehhalt, M. Endemann, J. M. Flaud, R. Gessner, A. Kleinert, R. Koopmann, J. Langen, M. López-Puertas, P. Mosner, H. Nett, H. Oelhaf, G. Perron, J. Remedios, M. Ridolfi, G. Stiller, and R. Zander (2008), MIPAS: an instrument for atmospheric and climate research, *Atmos. Chem. Phys.*, *8*, 2151–2188.

France, J. A., and V. L. Harvey (2013), A climatology of the stratopause in WACCM and the zonally asymmetric elevated stratopause, *Journal of Geophysical Research (Atmospheres)*, *118*, 2241–2254, doi:10.1002/jgrd.50218.

France, J. A., V. L. Harvey, C. E. Randall, R. L. Collins, A. K. Smith, E. D. Peck, and X. Fang (2015), A climatology of planetary wave-driven mesospheric inversion layers in the extratropical winter, *Journal of Geophysical Research (Atmospheres)*, *120*(2), 399–413, doi:10.1002/2014JD022244.

Funke, B., M. López-Puertas, M. García-Comas, G. P. Stiller, T. von Clarmann, M. Höpfner, N. Glatthor, U. Grabowski, S. Kellmann, and A. Linden (2009), Carbon monoxide distributions from the upper troposphere to the mesosphere inferred from 4.7 μm non-local thermal equilibrium emissions measured by MIPAS on Envisat, *Atmos. Chem. Phys.*, *9*(7), 2387–2411.

Funke, B., M. L. Puertas, L. Holt, C. E. Randall, G. P. Stiller, and T. von Clarmann (2014), Hemispheric distributions and interannual variability of NO_y produced by energetic particle precipitation in 2002-2012, *J. Geophys. Res.*, *119*(23), 13,565–13,582, doi:10.1002/2014JD022423.

García-Comas, M., B. Funke, A. Gardini, M. López-Puertas, A. Jurado-Navarro, T. von Clarmann, G. Stiller, M. Kiefer, C. D. Boone, T. Leblanc, B. T. Marshall, M. J. Schwartz, and P. E. Sheese (2014), Mipas temperature from the stratosphere to the lower thermosphere: Comparison of vM21 with ACE-FTS, MLS, OSIRIS, SABER, SOFIE and lidar measurements, *Atmos. Meas. Tech.*, *7*(11), 3633–3651, doi: 10.5194/amt-7-3633-2014.

García-Comas, M., M. López-Puertas, B. Funke, A. A. Jurado-Navarro, A. Gardini, G. P. Stiller, T. von Clarmann, and M. Höpfner (2016), Measurements of global distributions of polar mesospheric clouds during 2005–2012 by mipas/envisat, *Atmos. Chem. Phys.*, *16*(11), 6701–6719, doi:10.5194/acp-16-6701-2016.

Gelaro, R., W. McCarty, M. J. Suárez, R. Todling, A. Molod, L. Takacs, C. A. Rand les, A. Darmenov, M. G. Bosilovich, and R. Reichle (2017), The Modern-Era Retrospective Analysis for Research and Applications, Version 2 (MERRA-2), *Journal of Climate*, *30*(14), 5419–5454, doi:10.1175/JCLI-D-16-0758.1.

Global Modeling and Assimilation Office (GMAO) (2015), MERRA-2 inst3_3d_asm_Np: 3d, 3-Hourly, Instantaneous, Pressure-Level, Assimilation, Assimilated Meteorological Fields V5.12.4, doi:10.5067/QBZ6MG944HW0, Greenbelt, MD, USA, Goddard Earth Sciences Data and Information Services Center (GES DISC), Accessed: July 2019.

Hitchcock, P., and T. G. Shepherd (2013), Zonal-Mean Dynamics of Extended Recoveries from Stratospheric Sudden Warmings, *Journal of Atmospheric Sciences*, *70*, 688–707, doi:10.1175/JAS-D-12-0111.1.

Holt, L. A., C. E. Randall, E. D. Peck, D. R. Marsh, A. K. Smith, and V. Lynn Harvey (2013), The influence of major sudden stratospheric warming and elevated stratopause events on the effects of energetic particle precipitation in waccm, *J. Geophys. Res.*, doi:10.1002/2013JD020294.

Limpasuvan, V., Y. J. Orsolini, A. Chandran, R. R. Garcia, and A. K. Smith (2016), On the composite response of the MLT to major sudden stratospheric warming events with elevated stratopause, *Journal of Geophysical Research (Atmospheres)*, *121*, 4518–4537, doi:10.1002/2015JD024401.

Livesey, N. J., W. G. Read, P. A. Wagner, L. Froidevaux, A. Lambert, G. L. Manney, L. F. Millán-Valle, H. C. Pumphrey, M. L. Santee, M. J. Schwartz, S. Wang, R. A. Fuller, R. F. Jarnot, B. W. Knosp, and E. Martinez (2017), Version 4.2x Level 2 data quality and description document, *Tech. Rep. Tech. Rep. JPL D-33509 Rev. C*, Jet Propulsion Lab.

Lossow, S., F. Khosrawi, G. E. Nedoluha, F. Azam, K. Bramstedt, J. P. Burrows, B. M. Dinelli, P. Eriksson, P. J. Espy, M. García-Comas, J. C. Gille, M. Kiefer, S. Noël, P. Raspollini, W. G. Read, K. H. Rosenlof, A. Rozanov, C. E. Sioris, G. P. Stiller, K. A. Walker, and K. Weigel (2017), The SPARC water vapour assessment II: comparison of annual, semi-annual and quasi-biennial variations in stratospheric and lower mesospheric water vapour observed from satellites, *Atmospheric Measurement Techniques*, *10*, 1111–1137, doi:10.5194/amt-10-1111-2017.

Manney, G. L., W. A. Lahoz, J. L. Sabutis, A. O'Neill, and L. Steenman-Clark (2002), Simulations of fall and early winter in the stratosphere, *Quarterly Journal of the Royal Meteorological Society*, *128*(585), 2205–2237, doi:10.1256/qj.01.88.

Manney, G. L., K. Krüger, J. L. Sabutis, S. A. Sena, and S. Pawson (2005), The remarkable 2003–2004 winter and other recent warm winters in the Arctic stratosphere since the late 1990s, *J. Geophys. Res.*, *110*(D4), D04107, doi:10.1029/2004JD005367.

Manney, G. L., K. Krueger, S. P. K. Minschwaner, M. J. Schwartz, W. Daffer, N. J. Livesey, M. G. Mlynczak, E. Remsberg, J. M. Russell, and J. W. Waters (2008), The evolution of the stratopause during the 2006 major warming: Satellite Data and Assimilated Meteorological Analyses, *J. Geophys. Res.*, *113*, D11115, doi:10.1029/2007JD009097.

Manney, G. L., M. J. Schwartz, K. Krüger, M. L. Santee, S. Pawson, J. N. Lee, W. H. Daffer, R. A. Fuller, and N. J. Livesey (2009), Aura microwave limb sounder observations of dynamics and transport during the record-breaking 2009 arctic stratospheric major warming, *Geophys. Res. Lett.*, *36*.

Maury, P., C. Claud, E. Manzini, A. Hauchecorne, and P. Keckhut (2016), Characteristics of stratospheric warming events during northern winter, *Journal of Geophysical Research*, *121*(10), 5368–5380, doi:10.1002/2015JD024226.

Orsolini, Y. J., V. Limpasuvan, K. Pérot, P. Espy, R. Hibbins, S. Lossow, K. Raaholt Larsson, and D. Murtagh (2017), Modelling the descent of nitric oxide during the elevated stratopause event of January 2013, *Journal of Atmospheric and Solar-Terrestrial Physics*, *155*, 50–61, doi:10.1016/j.jastp.2017.01.006.

Randall, C. E., V. L. Harvey, G. L. Manney, Y. J. Orsolini, M. Codrescu, C. Sioris, S. Brohede, C. S. Haley, L. L. Gordley, J. M. Zawodny, and J. M. Russell III (2005), Stratospheric effects of energetic particle precipitation in 2003–2004, *Geophys. Res. Lett.*, *32*, L05802, doi:10.1029/2004GL022003.

Randall, C. E., V. L. Harvey, D. E. Siskind, J. France, P. F. Bernath, C. D. Boone, and K. A. Walker (2009), NO_x descent in the Arctic middle atmosphere in early 2009, *Geophys. Res. Lett.*, *36*, doi:10.1029/2009GL039706.

Ren, S., S. Polavarapu, S. R. Beagley, Y. Nezlin, and Y. J. Rochon (2011), The impact of gravity wave drag on mesospheric analyses of the 2006 stratospheric major warming, *Journal of Geophysical Research (Atmospheres)*, *116*, D19,116, doi:10.1029/2011JD015943.

Schranz, F., J. Hagen, G. Stober, K. Hocke, A. Murk, and N. Kämpfer (2019), Small-scale variability of stratospheric ozone during the ssw 2018/2019 observed at ny-alesund, svalbard, *Atmospheric Chemistry and Physics Discussions*, *2019*, 1–25, doi:10.5194/acp-2019-1093.

Schwartz, M. J., D. E. Waliser, B. Tian, D. L. Wu, J. H. Jiang, and W. G. Read (2008), Characterization of MJO-related upper tropospheric hydrological processes using MLS, *Geophys. Res. Lett.*, *35*, L08812, doi:10.1029/2008GL033675.

Siskind, D. E., S. D. Eckermann, J. P. McCormack, L. Coy, K. W. Hoppel, and N. L. Baker (2010), Case studies of the mesospheric response to recent minor, major, and extended stratospheric warmings, *Journal of the Atmospheric Sciences*, *115*(D3), doi:10.1029/2010JD014114, d00N03.

Smith, A. K., M. López-Puertas, M. García-Comas, and S. Tukiainen (2009), SABER observations of mesospheric ozone during NH late winter 2002-2009, *Geophys. Res. Lett.*, *36*, L23804, doi:10.1029/2009GL040942.

von Clarmann, T., M. Höpfner, S. Kellmann, A. Linden, S. Chauhan, U. Grabowski, B. Funke, N. Glatthor, M. Kiefer, T. Schieferdecker, , and G. P. Stiller (2009), Retrieval of temperature H_2O, O_3, HNO_3, CH_4, N_2O and $ClONO_2$ from MIPAS reduced resolution nominal mode limb emission measurements, *Atmos. Meas. Tech.*, *2*, 159–175.

Wang, L., and W. Chen (2010), Downward Arctic Oscillation signal associated with moderate weak stratospheric polar vortex and the cold December 2009, *Geophys. Res. Lett.*, *37*(9), L09707, doi:10.1029/2010GL042659.

Yamashita, C., S. L. England, T. J. Immel, and L. C. Chang (2013), Gravity wave variations during elevated stratopause events using saber observations, *J. Geophys. Res.*, *118*(11), 5287–5303, doi:10.1002/jgrd.50474.

Yigit, E., and A. Medvedev (2016), Role of gravity waves in vertical coupling during sudden stratospheric warmings, *Geoscience Letters*, *3*(1), doi:10.1186/s40562-016-0056-1.

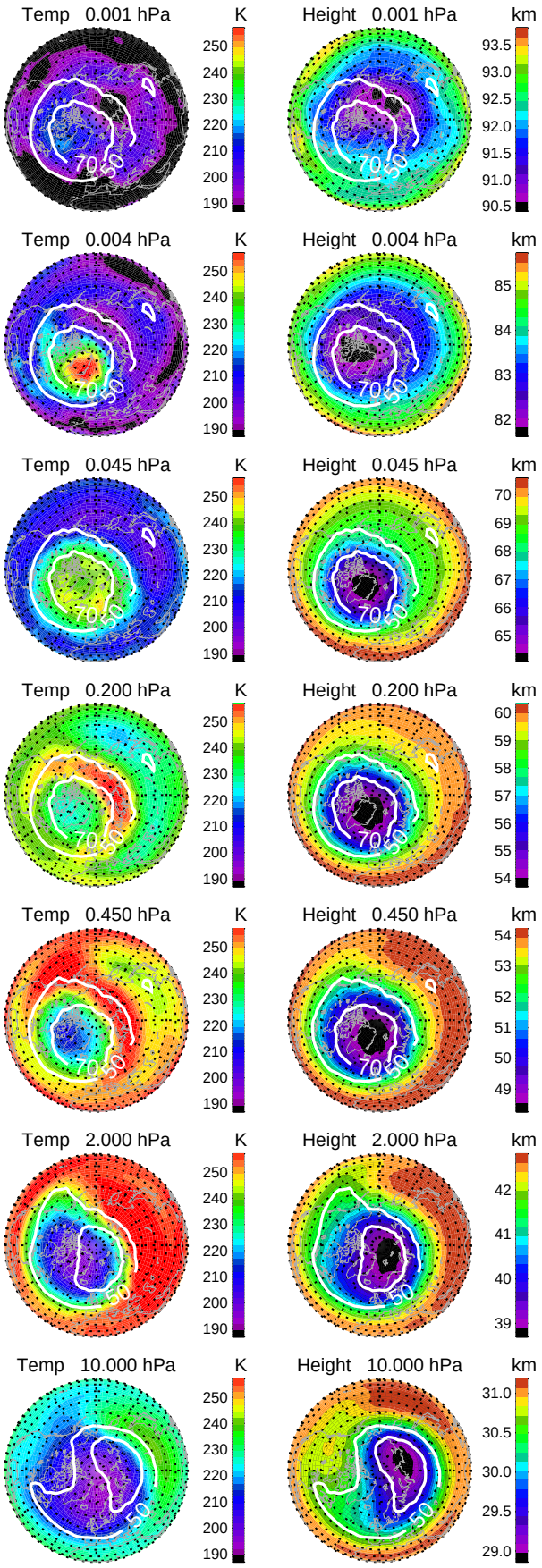

Figure 1. MIPAS temperature and altitude horizontal cross-section for November 29^{th} 2009. White contours show equivalent latitudes. Equivalent latitudes at 0.2 hPa and lower pressures correspond to those at 0.1 hPa.

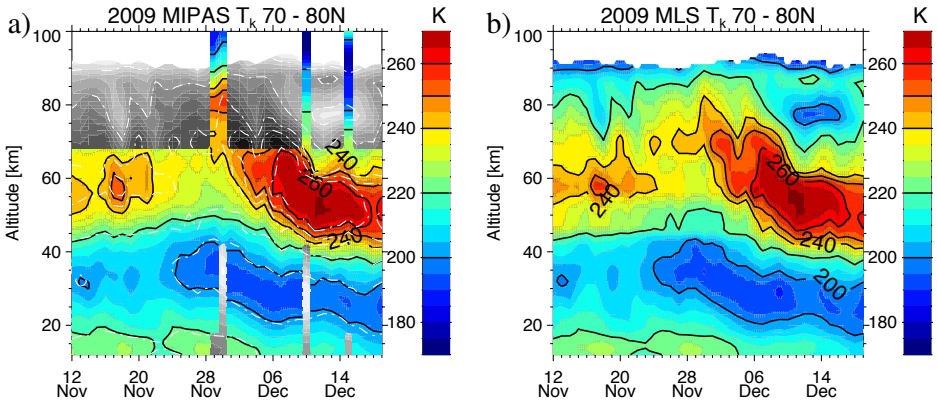

Figure 2. MIPAS (a) and MLS (b) temperature time series at 10°-80°W longitude and 70°N-80°N for late Autumn 2009. White dashed-contours and grey scale on the left plot correspond to the MLS data shown on the right plot. Y-axis in the right panel shows MIPAS altitudes at the corresponding MLS pressures. Black lines in color bars indicate the contour values.

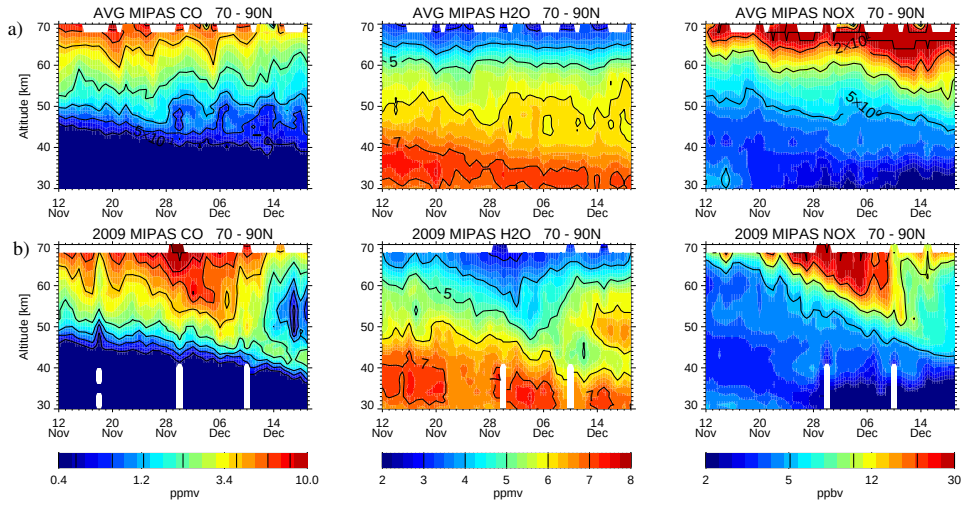

Figure 3. Early winter CO (left), H_2O (middle) and NO_x (right) time series at 70°-90°N equivalent latitude. Upper row: MIPAS 2007-2011 climatology (excluding 2009); lower row: MIPAS for 2009. Missing data is shown in white.

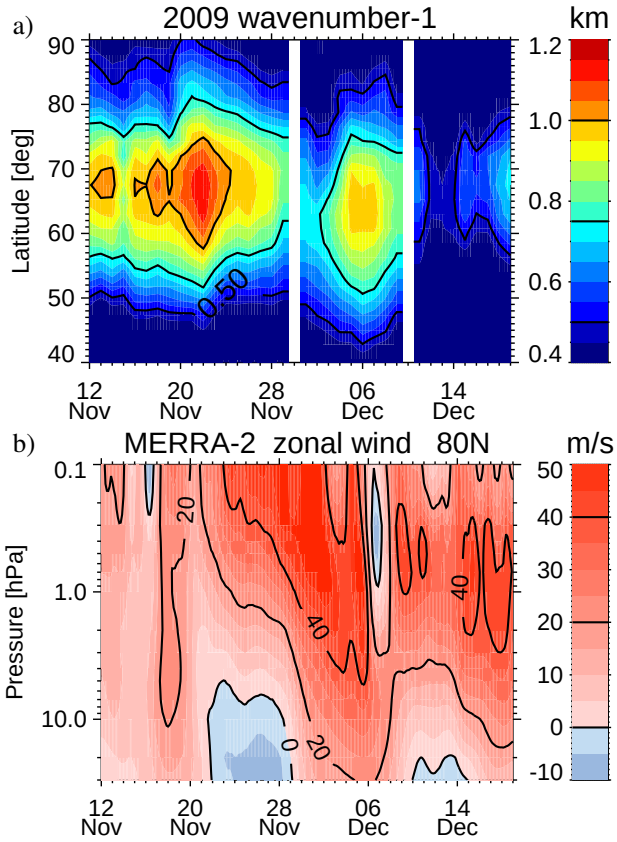

Figure 4. Upper panel: MIPAS height wavenumber-1 amplitudes at 10 mb in November-December 2009. Lower panel: MERRA-2 zonal mean zonal wind at 80°N averaged over a 4° latitude box from November to December 2009.

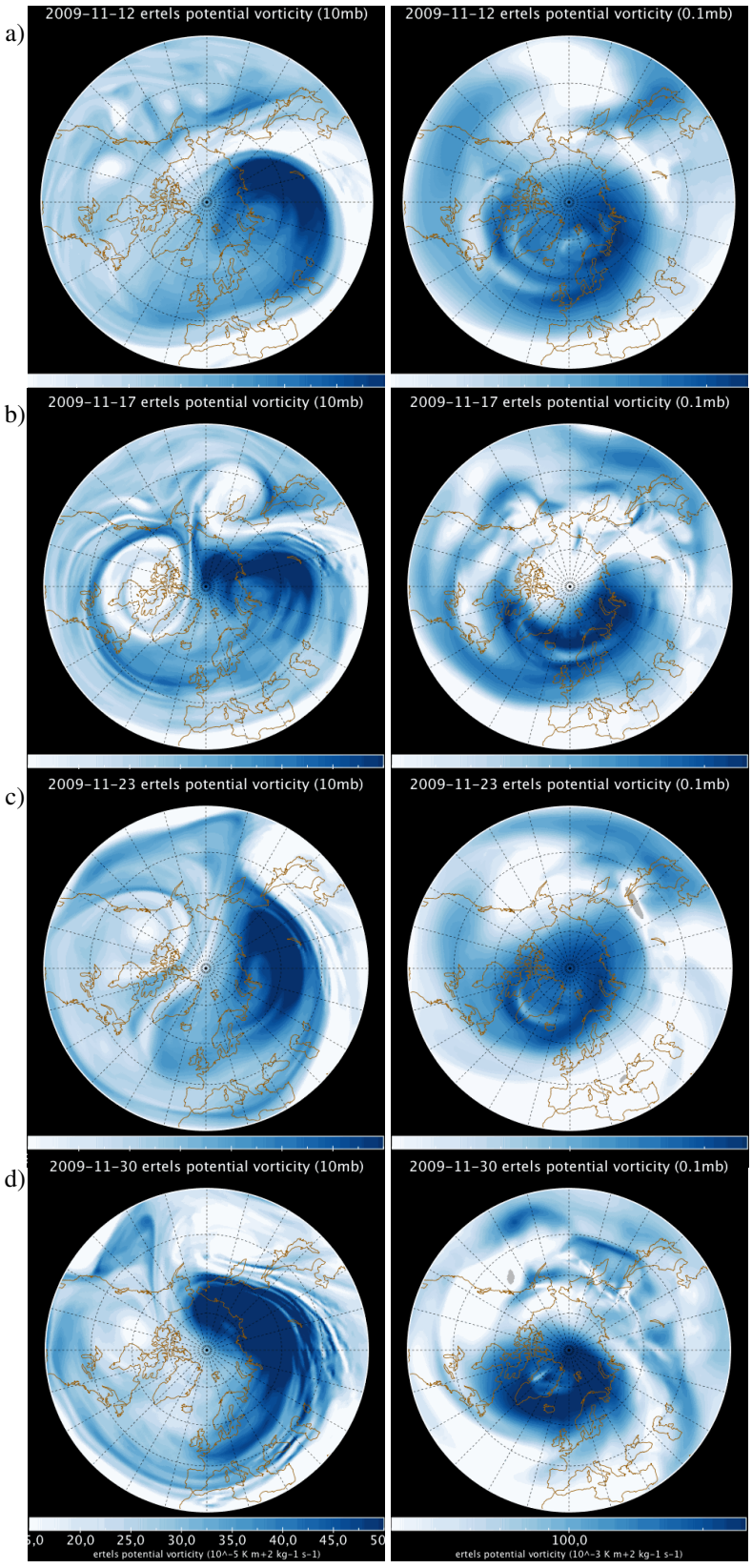

Figure 5. Merra-2 Ertel's potential vorticity for November 12^{th} (a), 17^{th} (b),23^{rd} (c) and 30^{th} 2009 (d) at 10 mb (left) and 0.1 mb (right).

Figure 1.

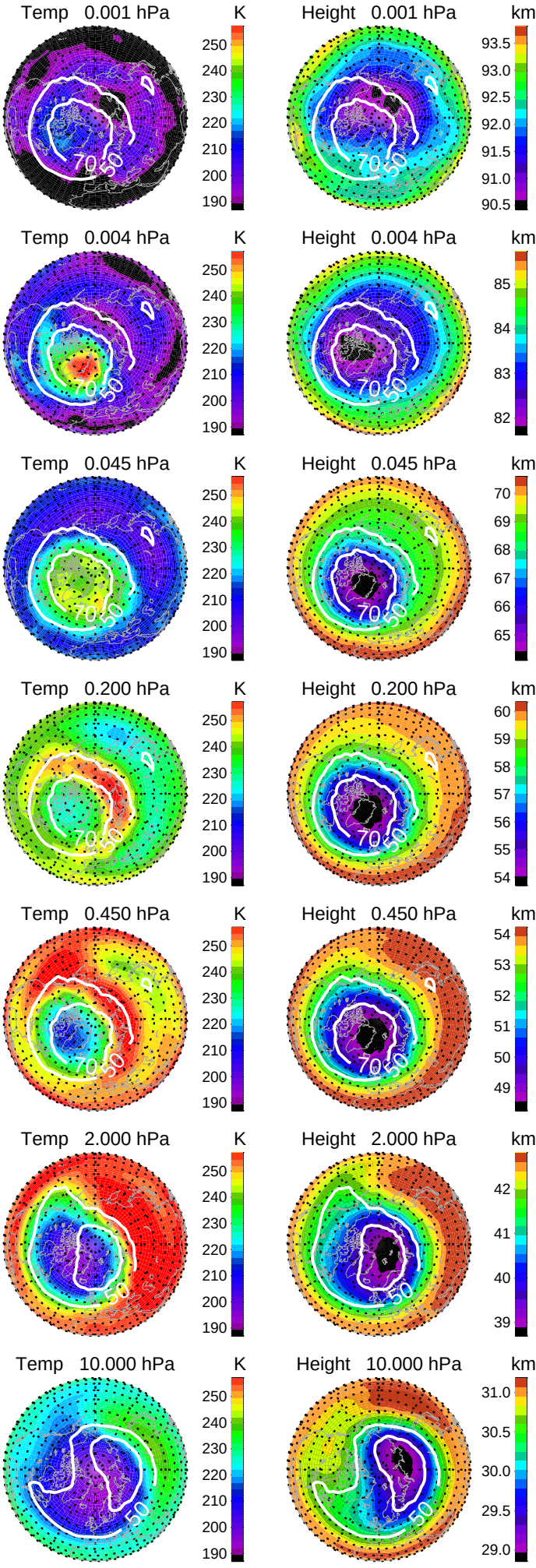
Temp 0.001 hPa
K
250
240
230
220
210
200
190
70
50
Height 0.001 hPa
km
93.5
93.0
92.5
92.0
91.5
91.0
90.5
Temp 0.004 hPa
K
Height 0.004 hPa
km
85
84
83
82
Temp 0.045 hPa
K
Height 0.045 hPa
km
70
69
68
67
66
65
Temp 0.200 hPa
K
Height 0.200 hPa
km
60
59
58
57
56
55
54
Temp 0.450 hPa
K
Height 0.450 hPa
km
54
53
52
51
50
49
Temp 2.000 hPa
K
Height 2.000 hPa
km
42
41
40
39
Temp 10.000 hPa
K
Height 10.000 hPa
km
31.0
30.5
30.0
29.5
29.0

Figure 2.

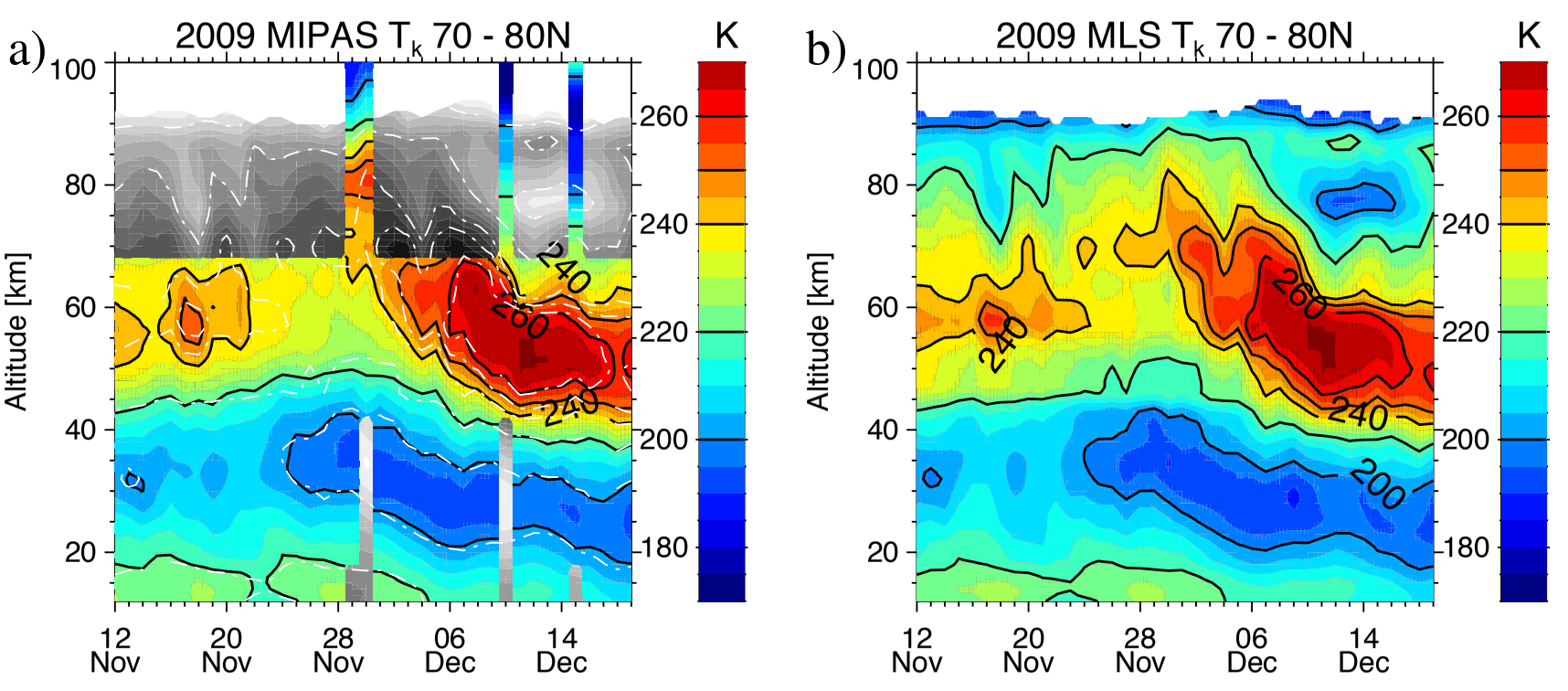
a)
2009 MIPAS T_k 70 - 80N
K
Altitude [km]
100
80
60
40
20
260
240
220
200
180
240
260
240
12 Nov
20 Nov
28 Nov
06 Dec
14 Dec
b)
2009 MLS T_k 70 - 80N
K
Altitude [km]
100
80
60
40
20
260
240
220
200
180
240
260
240
200
12 Nov
20 Nov
28 Nov
06 Dec
14 Dec

Figure 3.

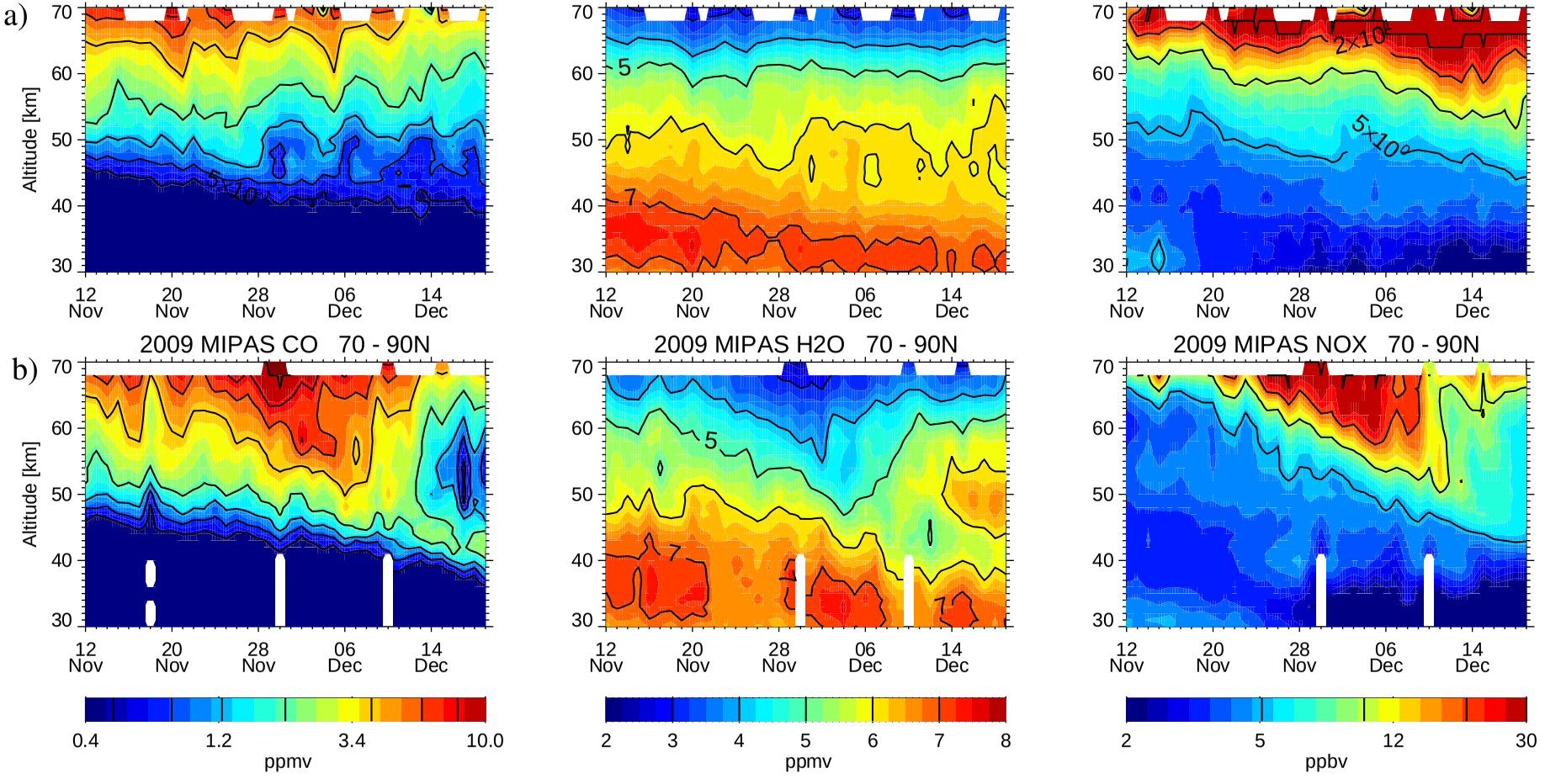
a)
AVG MIPAS CO 70 - 90N
AVG MIPAS H2O 70 - 90N
AVG MIPAS NOX 70 - 90N
b)
2009 MIPAS CO 70 - 90N
2009 MIPAS H2O 70 - 90N
2009 MIPAS NOX 70 - 90N
Altitude [km]
70
60
50
40
30
12 Nov
20 Nov
28 Nov
06 Dec
14 Dec
5x10
2x10
5
7
0.4
1.2
3.4
10.0
ppmv
2
3
4
5
6
7
8
ppmv
2
5
12
30
ppbv

Figure 4.

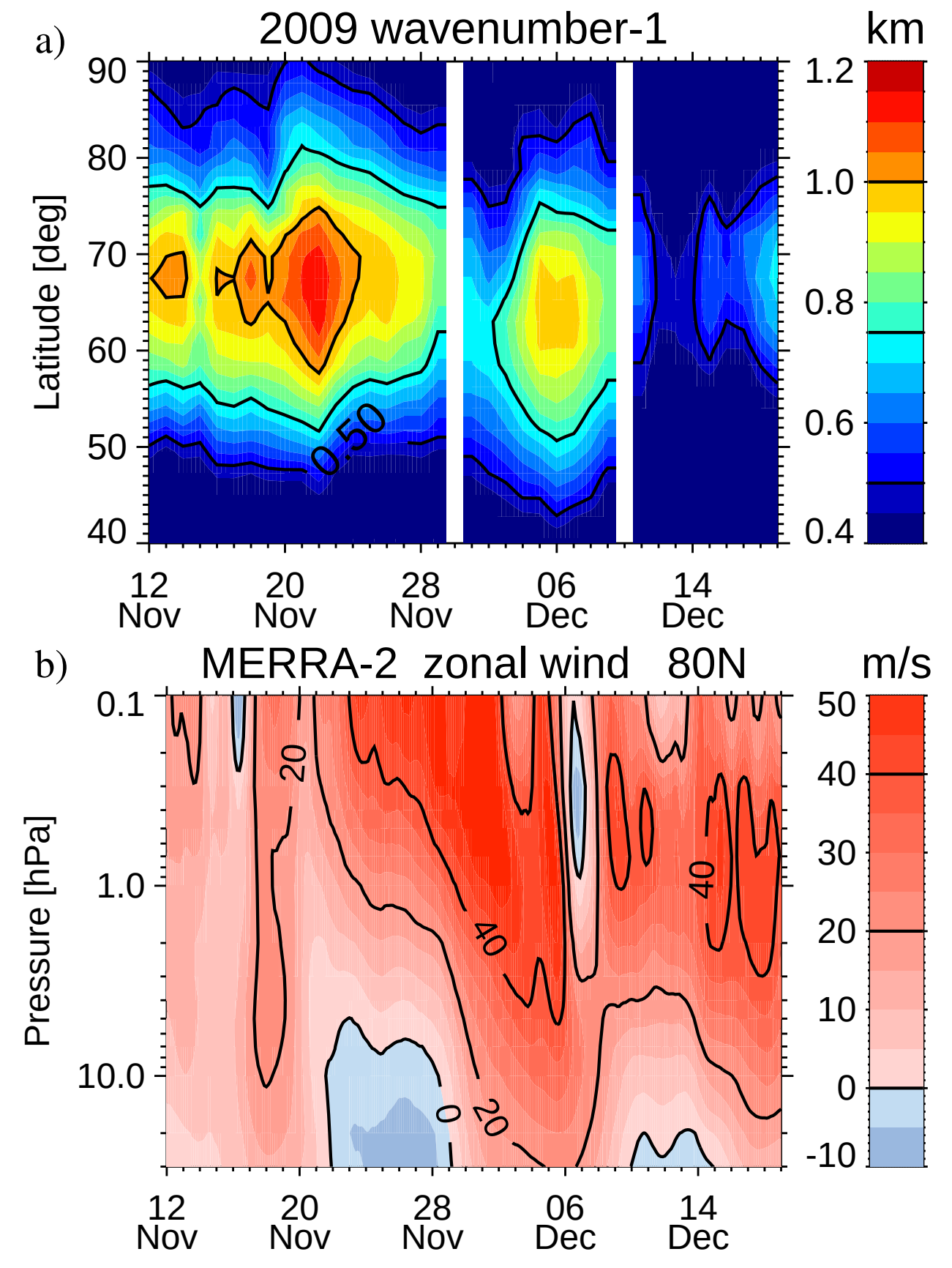
a)
2009 wavenumber-1
km
Latitude [deg]
90
80
70
60
50
40
0.50
1.2
1.0
0.8
0.6
0.4
12 Nov
20 Nov
28 Nov
06 Dec
14 Dec
b)
MERRA-2 zonal wind 80N
m/s
Pressure [hPa]
0.1
1.0
10.0
20
40
0
-20
50
40
30
20
10
0
-10
12 Nov
20 Nov
28 Nov
06 Dec
14 Dec

Figure 5.

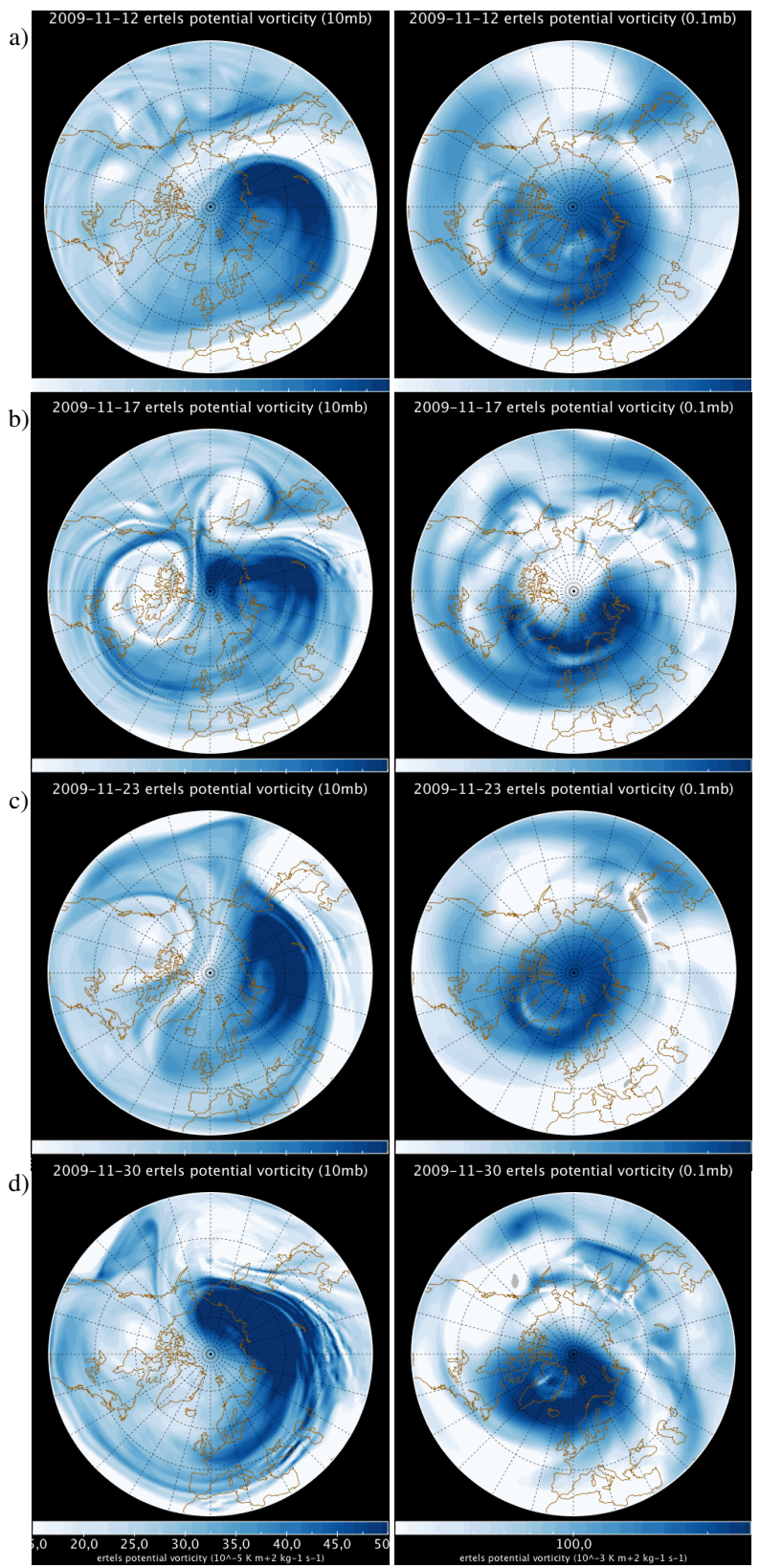
a)
2009-11-12 ertels potential vorticity (10mb)
2009-11-12 ertels potential vorticity (0.1mb)
b)
2009-11-17 ertels potential vorticity (10mb)
2009-11-17 ertels potential vorticity (0.1mb)
c)
2009-11-23 ertels potential vorticity (10mb)
2009-11-23 ertels potential vorticity (0.1mb)
d)
2009-11-30 ertels potential vorticity (10mb)
2009-11-30 ertels potential vorticity (0.1mb)
20,0 25,0 30,0 35,0 40,0 45,0 50
ertels potential vorticity (10^-5 K m+2 kg-1 s-1)
100,0
ertels potential vorticity (10^-3 K m+2 kg-1 s-1)